# THE EFFICIENCY OF HYBRID STEPPING MOTORS

## Analyzing the impact of control algorithms

BY STIJN DERAMMELAERE, BRAM VERVISCH, JOHANNES COTTYN, BART VANWALLEGHEM, PETER COX, FREDERIK DE BELIE, KURT STOCKMAN, LIEVEN VANDEVELDE, & GRIET VAN DEN ABEELE

STEPPING MOTORS ARE USED IN numerous applications because of their low manufacturing cost and simple open-loop position control capabilities. It is well known that their energy efficiency is low, although the actual efficiency values are generally not available. Moreover, the bulk of the stepping motors are driven in a nonoptimal way, e.g., in an open loop with a maximum current to avoid step loss and, thus, with low efficiency. In this article, the impact of the control algorithm on the efficiency of the motor is analyzed, measured, and discussed. The basic open-loop full-, half-, and microstepping algorithms are considered together with a more advanced vector control algorithm. For each algorithm, the torque/current optimization is discussed.

Stepping motors are typically used for multiple torque and speed operating points. To represent the efficiency of the motor at every operating point, isoefficiency curves are

*Digital Object Identifier 10.1109/MIAS.2013.2288403*
*Date of publication: 23 April 2014*

used. With these curves, the efficiencies of the motor, driven by different control strategies, can be compared.

## The Energy Efficiency of Stepping Motor Applications

Stepping motors are applied in the robotics, automotive, textile, and domestic apparatus industries, among many others. Their simple and cheap construction, ease of control, and open-loop capabilities make these motors very interesting in low-power applications. In addition, the absence of rotor windings reduces the inertia and weight so that high dynamics can be reached. Compared with dc-brush motors, the lack of contact aging serves the reliability and mechanical ruggedness. Finally, the availability of torque at a standstill makes a stepping motor perfectly suited for diverse applications.

However, despite all of these advantages, stepping motor control algorithms, such as open-loop, full-step control, result in very poor torque/current ratios. These low torque/current ratios are reflected in a low overall efficiency [1]. Nowadays, research on energy-efficient electrical machines focuses on induction machines because of their great share in the consumed energy [2]–[5]. On the other hand, the energy efficiency of fractional horsepower drives, such as stepping motors, is unaddressed in the literature. Moreover, as these motors are frequently used for low-power position control, the efficiency seems to be irrelevant. However, the worldwide market for stepping motors is estimated at 17% of the total market for motor drivers [6]. It is obvious that the total amount of stepping motors installed worldwide is enormous.

In general, stepping motors will operate continuously or intermittently, depending on the application. Especially in textile machines, stepping motors continuously consume energy. Therefore, it is obvious that assessing the energy consumption of stepping motors is very valuable for these applications. In automotive applications, stepping motors are used to position certain parts. Therefore, the stepping motor is operated for shorter periods. The total energy consumption and, therefore, the possible energy savings for these motors are rather low. However, in this article, it will be shown that the current needed to drive the motor can be significantly reduced, which is beneficial because the heat production will also be reduced. Furthermore, this reduction in the drive current will relieve the power electronics, the source, and the battery.

Basic open-loop drive algorithms, such as full, half, and microstepping, result in torque and speed ripples, noise, and vibrations [7]–[9]. The current stepping motor research focuses on more advanced motion control algorithms to suppress these vibrations and obtain smoother movements [10]–[13]. For this purpose, vector control algorithms, as used in permanent-magnet synchronous machines (PMSMs) and induction machines, are interesting to implement. Such a vector control algorithm also optimizes the torque dynamics of the motor [14], [15]. However, these vector control algorithms need rotor or flux position information to work properly. In most cases, the use of a mechanical position sensor is not the best option. Therefore, to implement vector control, sensorless control is a more interesting option. The research results concerning the control algorithms for PMSMs and induction machines are numerous [16]–[18]. Research efforts have been made to implement the latter control algorithms for stepping motors [19]–[21]. Some of these sensorless algorithms require machine models, which are described in [22] and [23]. However, using sensorless control for stepping motors is not very common. Most commercial drives do not allow for the measurement of the stator coil's voltage and current, which is essential to implement a sensorless control algorithm. Moreover, most stepper motor drives lack the computational power to implement an observer algorithm.

In this article, the efficiency of the basic and most popular open-loop drive methodologies, full, half, and microstepping, are analyzed and compared with a more advanced vector-control algorithm. As modern drives allow for the reduction of the current level for full-, half-, and microstepping profiles, these possibilities are analyzed to maximize the torque/current ratio. In this way, an overview of the efficiency, with respect to the control algorithm, of a two-phase hybrid stepping motor is given.

As stepping motors are typically used in a wide torque and speed range, the nominal efficiency values are not given. To present and assess the efficiency of the motor for different control strategies and various load profiles, isoefficiency curves are used [24]–[27]. With these curves, the efficiency of the different control strategies can be easily compared. Moreover, a dedicated test rig is also used to measure and compare the efficiency of seven different stepping motors at important operating points.

## Stepping Motor Torque Generation

The principle of operation of a two-phase hybrid stepping motor is illustrated in [22] and [23] and shown in Figure 1(a) and (b). The rotor is attracted by the excited stator phase. In Figure 2, the static torque-rotor position curves are plotted for both phases.

The motor torque contains an electrodynamic component, a cogging torque component due to the multitoothed construction and a component caused by the reluctance effect [28], [29]. The electrodynamic component generated by the interaction between the stator current and the permanent magnet rotor field is dominant, as stated in [30], and, hence, the torque-position curves can be modeled as

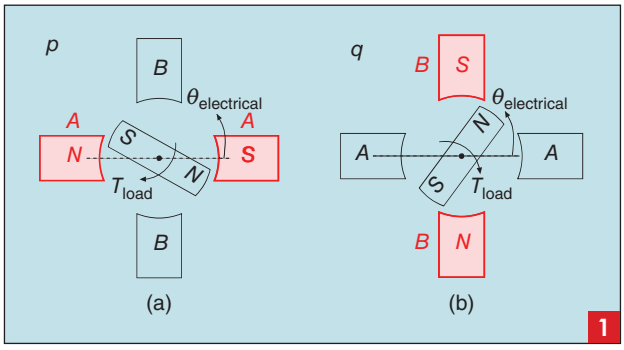


**The simplified motor construction and operating principle of a two-phase hybrid stepping motor. (a) *p*—phase A excited (red). (b) *q*—phase B excited (red).**

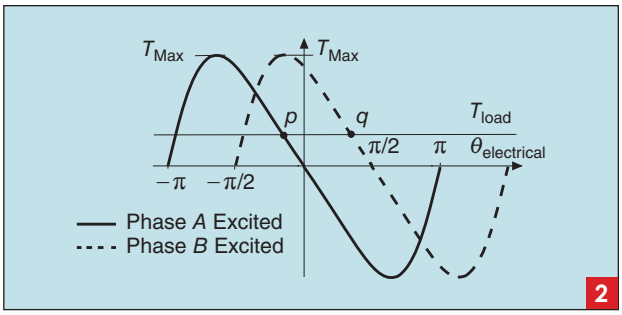


**The static torque-rotor position curves of a hybrid stepping motor.**

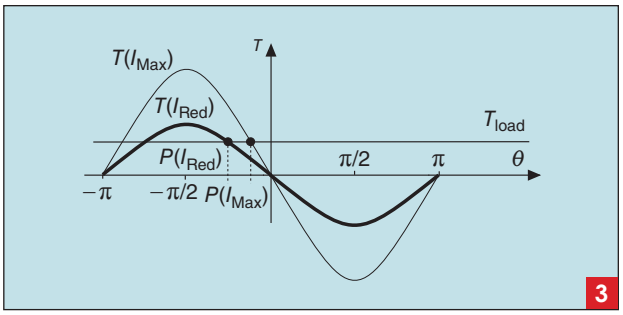


**Reducing the current to optimize the torque/current ratio.**

$$\begin{cases} T_a = -C_T \cdot I. \sin(\theta_{\text{electrical}}) \\ T_b = C_T \cdot I. \cos(\theta_{\text{electrical}}). \end{cases} \tag{1}$$

The solid curve in Figure 2 illustrates the static torque-position relation for an excited phase A. For a given load torque, $T_{\text{load}}$, a stable operating point, $p$, is reached. When a step (full-step mode) command is given, phase B will be excited and the excitation of phase A is removed. The dotted line illustrates the torque when phase B is excited. For the same load torque $T_{\text{load}}$, the rotor moves until a new equilibrium point, $q$, is reached.

As shown in (1), for an excited phase A, the maximum torque, for a given dc $I$ in phase A, is available at $\theta_{\text{electrical}} = -\pi/2$ rad. For the load torque in Figure 2, the equilibrium position of the rotor is $p$. At zero speed, the maximum torque related to the applied current is not used to hold the load. For this reason, a reduced current could be used to hold the same load torque, operating the machine at $\theta_{\text{electrical}} = -\pi/2$ rad. This method reduces the copper losses and, hence, increases the efficiency of the drive.

Figure 3 shows the effect of a current reduction on the torque-position curve. The current reduction results in a new equilibrium point. However, because of the high number of pole pairs, this change in the rotor position is, in most cases, not relevant. The minimum current to drive a mechanical load at a certain speed setpoint depends on the required torque. When the mechanical load is modeled as a constant load torque $T_{\text{load}}$, mechanical friction $b$, and an inertia $J$, the necessary motor torque $T_{\text{em}}$ can be written as

$$T_{\text{em}} = T_{\text{load}} + b \cdot \frac{d\theta}{dt} + J \cdot \frac{d^2\theta}{dt^2}. \tag{2}$$

When a regime situation is considered, the torque required to accelerate and decelerate the load can be neglected as in [31]. Hence, (2) simplifies and the average motor torque $\overline{T_{\text{em}}}$ is

$$\overline{T_{\text{em}}} = T_{\text{load}} + b \cdot \frac{d\theta}{dt}. \tag{3}$$

This average torque depends on the drive algorithms addressed in the following section.

## Stepping Motor Drive Algorithms

The stepping motor construction is ideally suited for open-loop positioning. When constant phase currents are applied, the rotor moves from one discrete steady-state position to another. By counting the step command pulses, open-loop positioning is made possible. In addition to the basic full-, half-, and microstepping algorithms, based on the discrete steady-state rotor positions, a more advanced vector control algorithm is discussed.

### *Full Step*

For the full-step algorithm, shown in Figure 4(a), only one phase at a time is excited. When a full-step command is given, the excitation of one phase is released, while another phase is excited. This results in rather large steps.

To determine the minimum current needed to move the load at a certain speed, the optimal torque usage is considered in Figure 4(a) on the right. This figure shows that phase B should be excited when $\theta_{\text{electrical}} \in [-\pi/4, \pi/4]$ to optimize the torque usage. When the angular position $\theta_{\text{electrical}}$ exceeds $\pi/4$, the excitation should be switched to $-$A. For this optimal situation, the average motor torque can be determined based on the interval $\theta_{\text{electrical}} \in [-\pi/4, \pi/4]$

$$\overline{T_{\text{em}}} = \frac{\int_{-\frac{\pi}{4}}^{\frac{\pi}{4}} C_T.I. \cos(\theta_{\text{electrical}}) d\theta}{\frac{\pi}{4} - -\frac{\pi}{4}}. \tag{4}$$

Solving (4) results in the optimal average full-step torque

$$\overline{T_{\text{em}}} = 0,90.C_T.I. \tag{5}$$

### *Half Step*

When both phases are excited simultaneously at the maximum current [Figure 4(b)], a stable operating point 1 between 0 and 2 is obtained. The step angle between two discrete operating points is half that of the full-step operation. This is called *half-step operation*. The half-step commands have to come twice as fast as the full-step commands to obtain the same rotational speed. Therefore, the $\theta_{\text{electrical}}$ interval, shown in the right part of Figure 4, in which one phase is excited changes from $\pi/2$ for full-step to $\pi/4$ in half-step operation. In the optimal situation, torque production is shown in the right part of Figure 4(b). Based on this figure and a similar calculation as in (4), the average torque can be determined for an optimal half-step operation

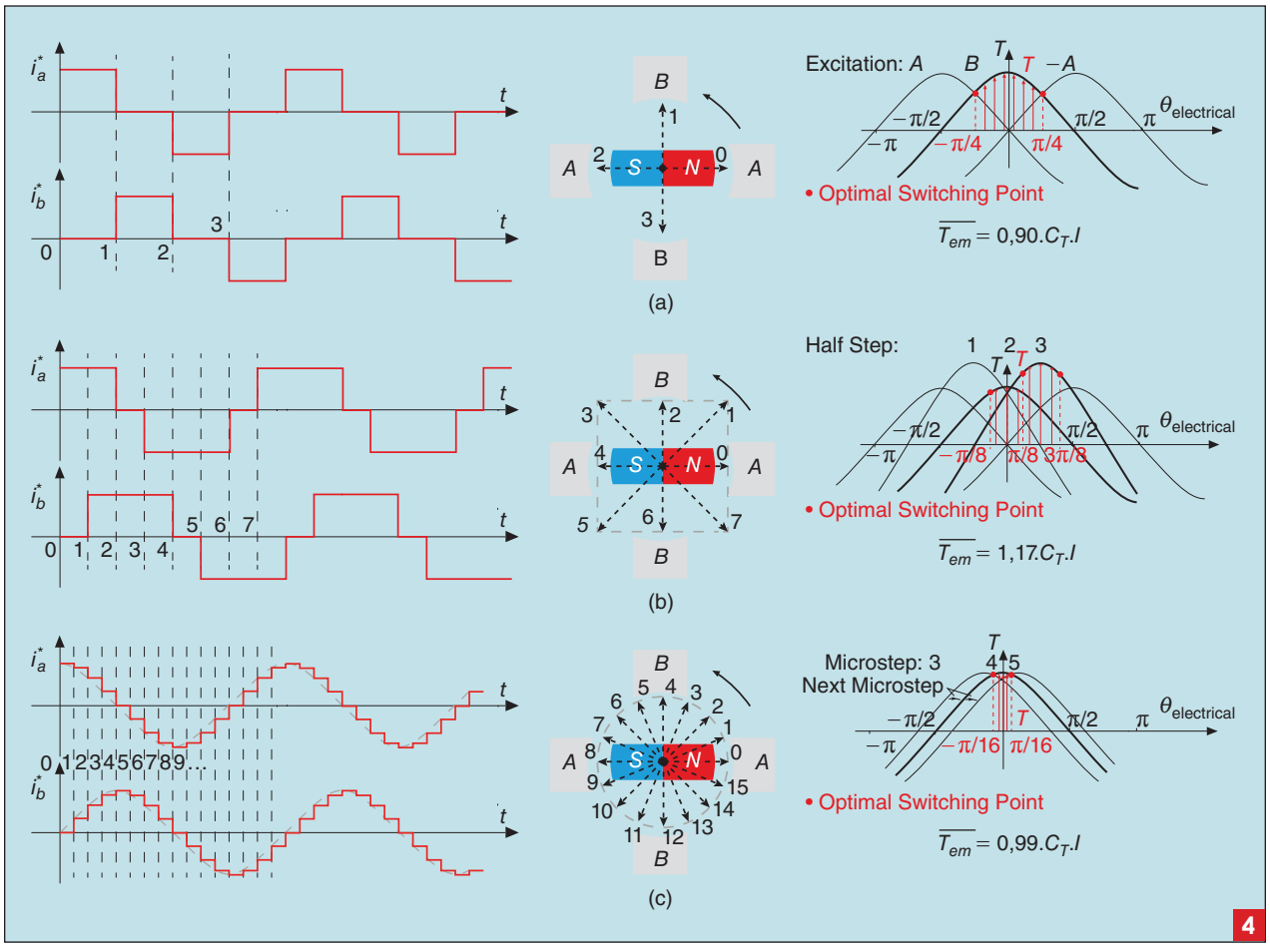


**The (a) full-, (b) half-, and (c) microstepping excitation schemes (left), stable rotor positions (middle), and optimal exitation interval (right).**

$$\overline{T_{\text{em}}} = C_T.I.\frac{\int_{-\frac{\pi}{8}}^{\frac{\pi}{8}} \cos(\theta)d\theta + \sqrt{2}.\int_{\frac{\pi}{8}}^{\frac{3\pi}{8}} \cos(\theta - \pi/4)d\theta}{\frac{3\pi}{8} - -\frac{\pi}{8}}. \quad (6)$$

The average torque $\overline{T_{\text{em}}} = 1{,}17.C_T.I$ is higher compared with the proposed full-step algorithm. However, the difference in torque production at each step results in a different position response, as shown in Figure 5.

### *Microstepping*

Finally, microstepping [Figure 4(c)] is based on additional current setpoints, which are a fraction of the maximum current. This approach makes it possible to further reduce the step angle. As the step angle decreases, the movement becomes smoother, as shown in Figure 5. The calculation of the average torque for the optimal current is similar to the calculation for the full step. The average torque of $\overline{T_{\text{em}}} = 0{,}99.C_T.I$ for a one-fourth microstep algorithm is higher than that of a full-step operation, and the constant torque production at each step guarantees a smoother operation.

When a stepping motor with a full-step angle of 1.8° has to be driven at 1,000 r/min with a 1/64th microstepping algorithm, the controller has to send a step command every 4.7 µs. The computational power of the controller limits the ability to divide a full step into smaller microsteps at higher speeds.

Another remark on the half- and microstepping approach concerns the accuracy. When phase A is excited as in Figure 2, the expected rotor position is $\theta_{\text{electrical}} = 0°$. Due to the load torque, the exact rotor position will deviate. However, when a full-step command is given, the rotor will still move to the next position according the step angle. The accuracy of the step-by-step movement will not be influenced by the full-, half-, or microstepping algorithm. The angular displacement after a step command will be constant for a constant load torque.

### *Vector Control*

Figure 6 shows the vector control principle. The flux vector $\Phi_R$ is fixed to the permanent-magnet rotor. The vector control algorithm requires that the two phases can be excited simultaneously. The combination of the currents in phase A and B results in the fundamental stator-current vector $\boldsymbol{i}_s$. When neglecting the reluctance and saturation effects, the torque can be written as

$$T_{\text{motor}} = C_T.i_s.\sin(\delta), \quad (7)$$

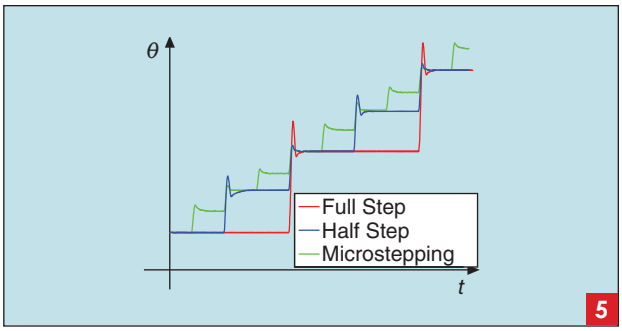


**The full-, half-, and microstepping rotor movement.**

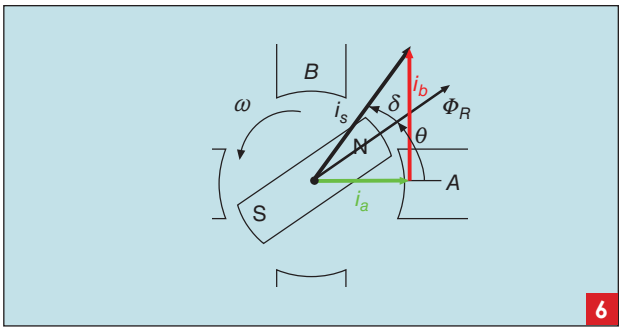


**The vector control torque generation.**

where the motor torque is proportional to the stator current vector amplitude and the sine of the load angle, $\delta$. The load angle $\delta$ is the angle between the stator current vector, $i_s$, the rotor flux vector, and the rotor flux vector $\Phi_R$. Neglecting the reluctance effect, the torque–current ratio is optimal when $\delta$ equals $\pi/2$. By applying a closed-loop controller, the load angle, $\delta$, can be controlled in a stable way.

The implementation of this vector control algorithm is shown in Figure 7. The setpoint currents $i_a^*$ and $i_b^*$ are computed to have a load angle, $\delta$, of $\pi/2$. The current amplitude, $i_s$, results in the required torque. The vector control principle proposed in [22] and shown in Figure 7 has a simple straightforward structure. However, when a sensorless position estimation algorithm is implemented, the computational cost will seriously increase.

## Efficiency of a Stepping Motor

The efficiency of a stepping motor is given by

$$\eta = \frac{P_{\text{out}}}{P_{\text{in}}} = \frac{P_{\text{mech}}}{P_{\text{mech}} + P_{\text{loss}}}. \tag{8}$$

The electric power supplied to the drive is converted into useful mechanical power as well as some electrical and mechanical losses. In general, the losses appearing in electric machines are copper, iron, friction and windage, and stray load [6]. Since the cooling is natural, there are no windage losses. As the stepping motors are situated in the low power range, the iron, friction, and stray load losses will be neglected. The measurements will show the error made by this simplification.

### *Copper Losses*

For the representation of the copper losses, the RMS value of the phase current is used. The copper losses in a phase, using the RMS currents, are

$$P_c = I_{\text{ph,RMS}}^2 \cdot R_{\text{ph}}. \tag{9}$$

The actual phase current for the different stepping modes follows the patterns plotted in Figure 4. The RMS value results in an equivalent dc, generating the same copper losses as the actual phase current. The RMS current is defined as

$$I_{\text{ph,RMS}} = \sqrt{\frac{1}{T}\int_0^T i_{\text{ph}}^2(t)\,dt}. \tag{10}$$

As shown in Figure 4, for a certain rotational speed, the signal period, $T$, will be the same for the different drive algorithms. Solving (10) for the full and half algorithms shown in Figure 4, the RMS current can be written as

$$I_{\text{ph,RMS}} = I_{\text{peak}} \cdot \sqrt{D}, \tag{11}$$

where $D$ is the duty cycle ($D = 0.5$ for a full step and $D = 0.75$ for a half step).

The RMS current for the microstepping algorithm depends on the number of microsteps. For the microstepping profile in Figure 4(c), which uses four microsteps, the RMS current is

$$I_{\text{ph,RMS}} = 0.74.I_{\text{peak}}. \tag{12}$$

The open-loop full-, half-, and microstepping algorithms use known current setpoints to drive the motor. If the closed-loop vector control algorithm is used, the current setpoint is continuously adapted. Therefore, a theoretical calculation of the efficiency for the closed-loop vector is impossible.

### *Theoretical Efficiency*

Considering the two phases of the stepping motor, the theoretical efficiency, assuming only copper losses, can be written as

$$\eta = \frac{P_{\text{out}}}{P_{\text{in}}} = \frac{P_{\text{mech}}}{P_{\text{mech}} + \left(I_{\text{ph,RMS}}^2 \cdot R_{\text{ph}}\right) \cdot 2}. \tag{13}$$

The peak current, $I_{\text{peak}}$, for the analyzed motor is 5.7 A and equals the nominal current of the motor. At the nominal motor temperature, each stator phase has a resistance of 0.65 Ω. With these specifications, the efficiency can be mapped in an isoefficiency curve (Figures 8–10). The contour lines indicate a variation of 2.5%, and the vertical color bar on the right side represents the efficiency, ranging from 0 to 80%. The maps are limited by the physical torque and speed limits of the drive system.

As shown in Figures 8–10, the efficiency of the stepping motor is very low. This is due to the high current, the relatively high phase resistance of the small motor, and the poor torque/current ratio. The half- and microstepping control result in an even lower efficiency due to the higher duty cycle. Although the exact measured efficiencies are discussed in the following section, these results are interesting as they identify the copper losses as the main reason for the low efficiency.

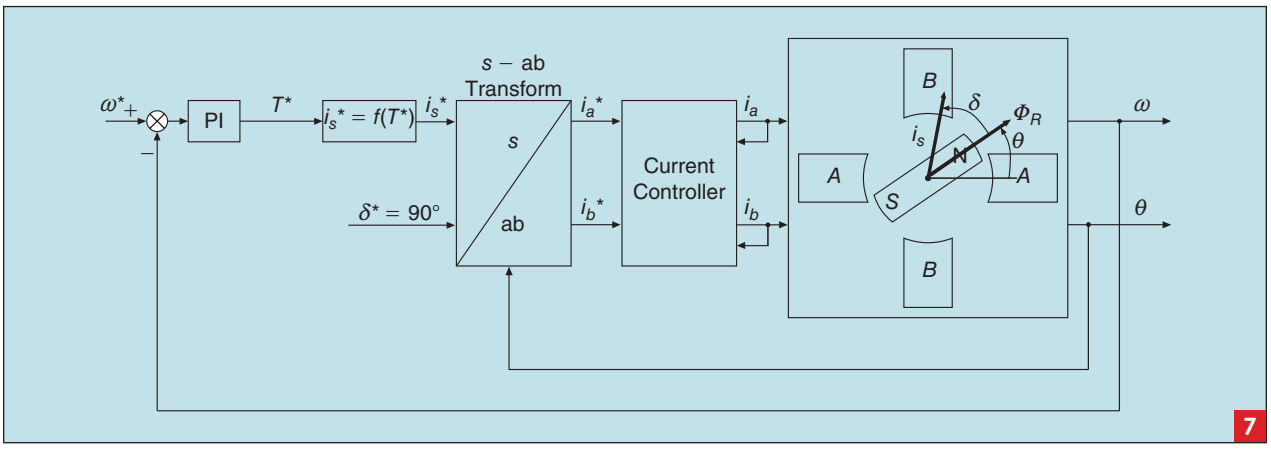


7

**The vector control implementation [22].**

The efficiency reaches its maximum when the product of the load torque and speed setpoint is at the maximum. This occurs in the upper right corner of the torque–speed operating area. However, in the "Stepping Motor Torque Generation" section, it was concluded that the desired torque can be achieved with a smaller current. By reducing the current, the losses can be reduced significantly in some operating areas.

## Measurements

The test rig that was used to measure the efficiency is shown in Figure 11. To calculate the efficiency, the current, $i_{dc}$, and voltage, $v_{dc}$, at the dc bus of the stepping motor drive are measured and sampled every 0.1 ms (Figure 12). The advantage of this approach is that the total amount of power that is necessary to drive the motor, including the switching losses of the power electronics, can be measured

$$P_{in} = \frac{1}{t}\int_0^t V_{dc} \cdot i_{dc}\, dt. \tag{14}$$

Then, the measured efficiency is computed by

$$\eta = \frac{P_{mech}}{P_{in}}. \tag{15}$$

The mechanical power is calculated by

$$P_{mech} = T \cdot \omega. \tag{16}$$

The torque, $T$, is measured by a torque sensor. The speed setpoint is known and verified by means of the encoder output.

Steady-state measurements are made at 55 different speed values and 25 different load torque values, resulting in a matrix of 1,375 measurement points for one motor. At certain operating points, the motor is not able to move the load at the given speed setpoint. These limits, which are clearly visible in the isoefficiency curves, are inherent to the mechanical parameters of the test bench, such as friction, and will vary compared with other applications.

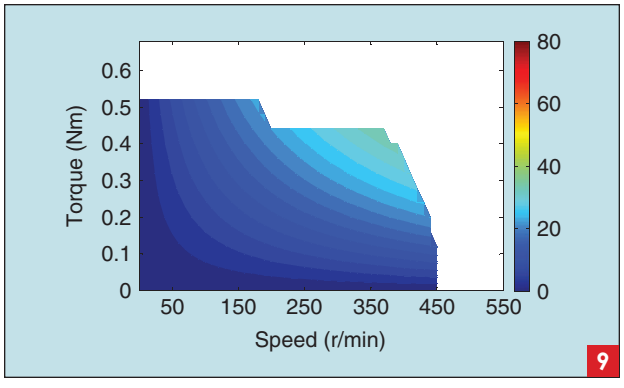


9

**The half-step theoretical efficiency (%) curve.**

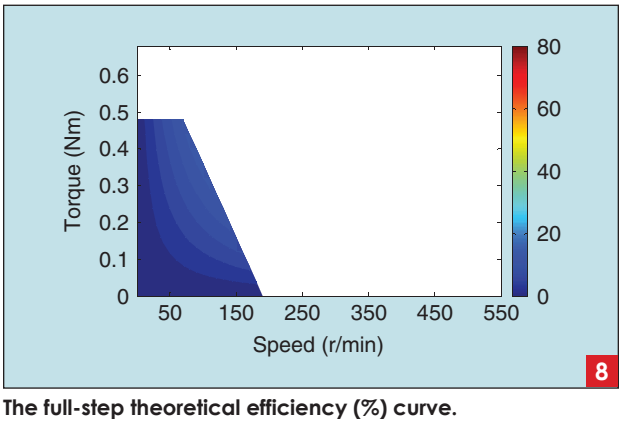


8

**The full-step theoretical efficiency (%) curve.**

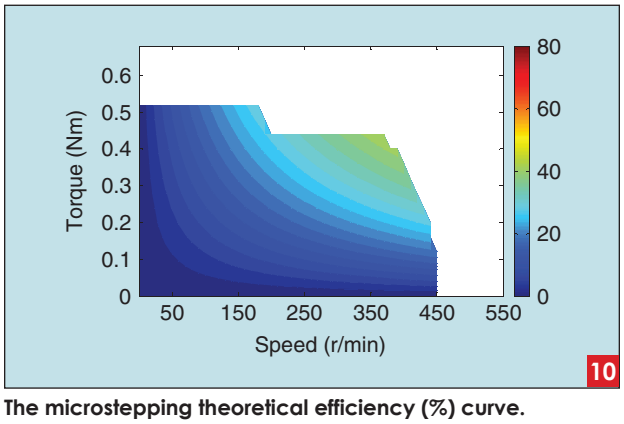


10

**The microstepping theoretical efficiency (%) curve.**

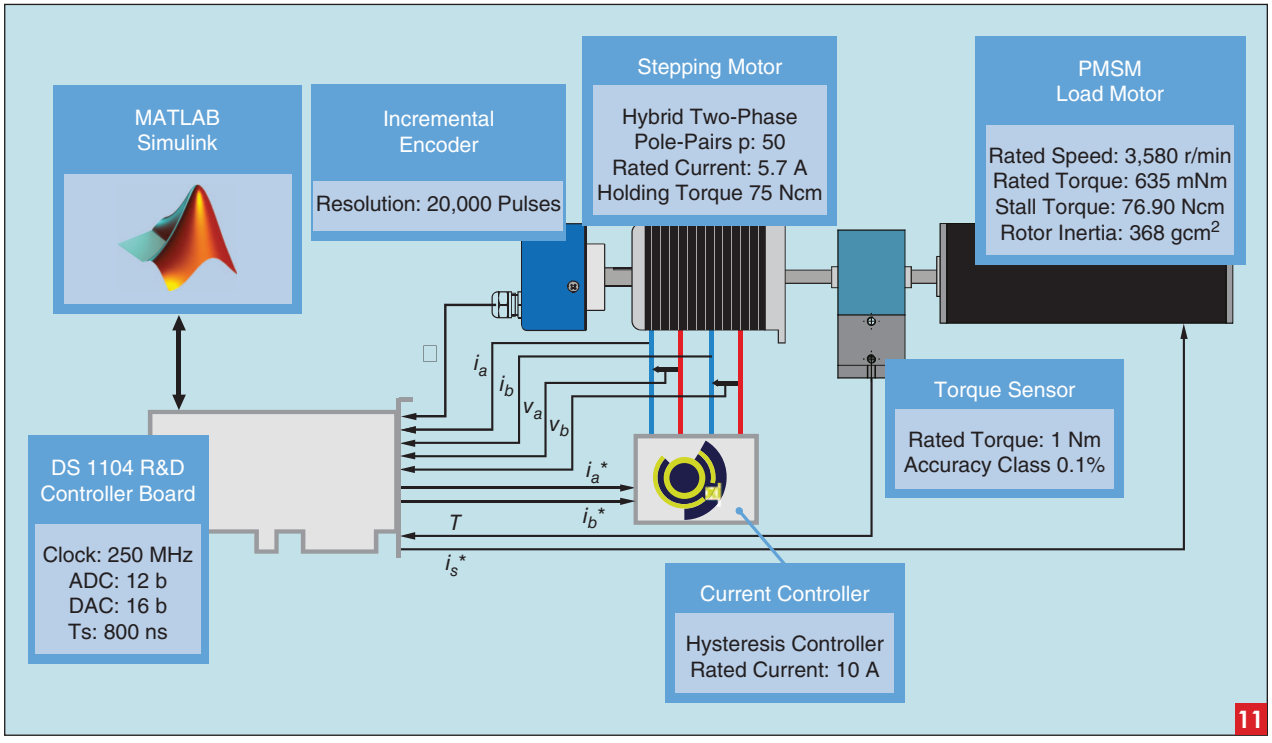


**The dedicated test rig used to measure the efficiency.**

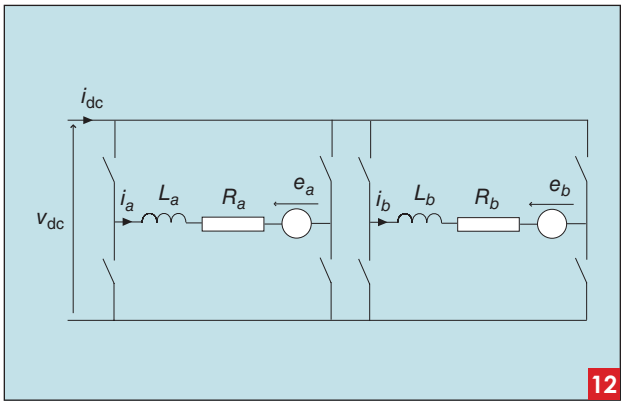


**The electric scheme and measurements with back-EMF signals $e_a$ and $e_b$.**

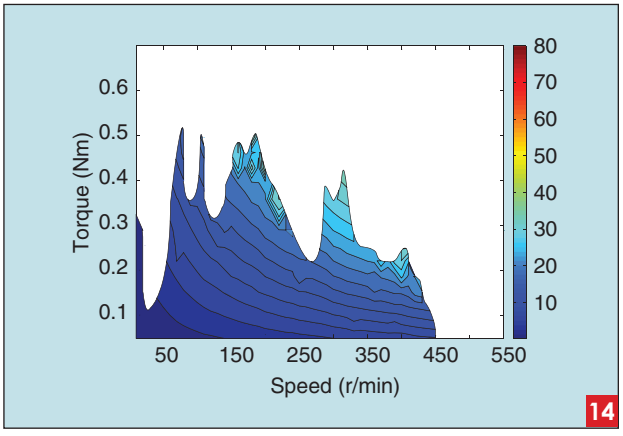


**The half-step measured efficiency (%) curve.**

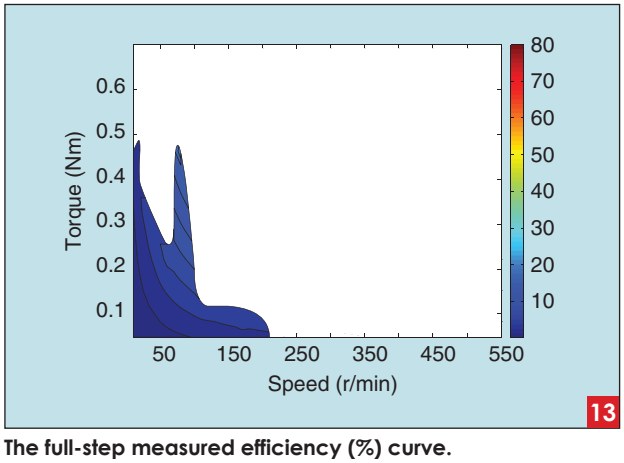


**The full-step measured efficiency (%) curve.**

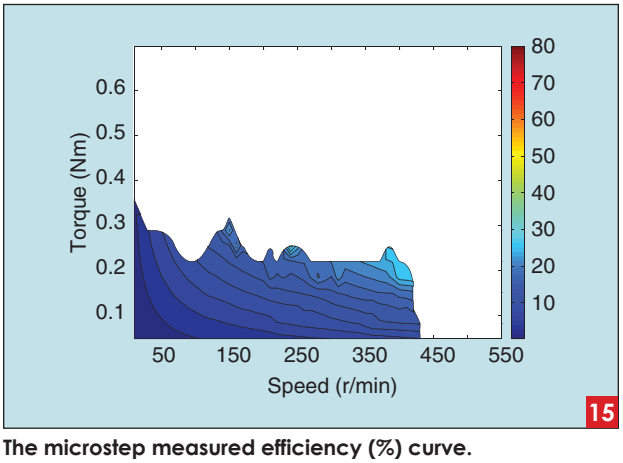


**The microstep measured efficiency (%) curve.**

Moreover, the dedicated test rig is also used to measure and compare the efficiency of seven different stepping motors at important operating points.

### *Nominal Current*

At first, the motor is driven at a nominal current. The isoefficiency curves for full, half, and microstepping are shown in Figures 13–15. The overall efficiency is a little lower than expected according to the theoretical approach, particularly at higher speeds. The maximum deviation between the theoretically calculated and measured efficiency is 3.5%. This can be due to iron, friction, and stray load losses. Furthermore, the currents generated by the drive are not exact square waves as assumed during the theoretical assessment. As a result, (11) shows an approximation of the computed RMS value of the current.

For the unipolar hysteresis current control used in this article, Figure 16 plots the currents in a single phase for different speeds. Current overshoot and oscillation occur when the current converges to zero. These oscillations increase the RMS value of the current. At low speeds, this ripple can be neglected as its duration is small compared with the excitation time, $t_{step}$. However, at higher speeds, it becomes more important. At 77 r/min [Figure 16(b)], the RMS current increases with 1% due to this effect. At 150 r/min, the RMS increase is already 3%. The increased RMS current produces higher copper losses compared with the theoretical approximation. The optimization of the current control algorithm will reduce these additional losses.

### *Current Reduction*

To measure the efficiency at more optimal current levels, the current for every torque/speed operating point is reduced to as low as possible, meaning to the lowest current at which the motor is still able to perform the movement at the setpoint speed. This implies that there is no margin for acceleration or torque disturbances. The measurement results are shown in Figures 17–19.

The maximum current reduction is determined by (4), and the optimal torque generation is shown in Figure 4 and in the "Steeping Motor Drive Algorithms" section. For low-speed setpoints and load torques, the current could be reduced significantly, as shown in Table 1. However, the losses at these operating points are relatively high compared with the mechanical power, resulting in a low efficiency. According to (5), the margin for a current reduction is low at high-speed setpoints and load torques. In conclusion, the efficiency can be maximized at half the maximum speed and torque, as shown in Figures 17–19 and in Table 1.

As predicted in the "Steeping Motor Drive Algorithms" section, the current reduction can be higher at half and microstepping because of the higher average torque available. This is shown in Figures 18 and 19, where the efficiencies are higher because of a further current reduction. Moreover, there are many more operating points at which the motor is able to operate smoothly in half and microstepping compared with full step. Figures 18 and 19 show better efficiencies than Figure 16. From Figures 13, 14, 17, and 18, it follows that the half-step drive methodology will only result in a higher efficiency if a current reduction is applied.

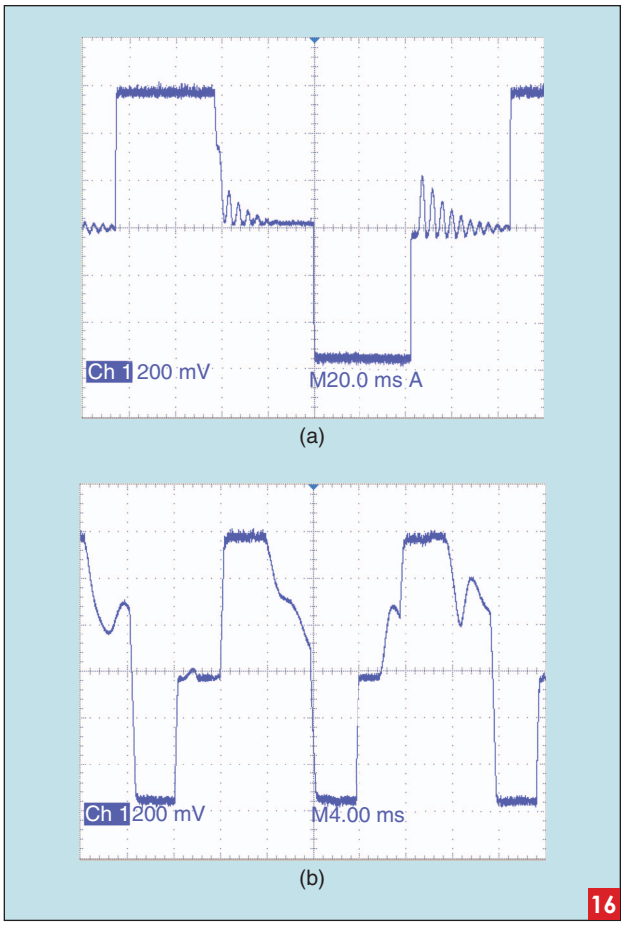


**The current in one phase (a) at 7 r/min and (b) at 77 r/min (100 mV/A).**

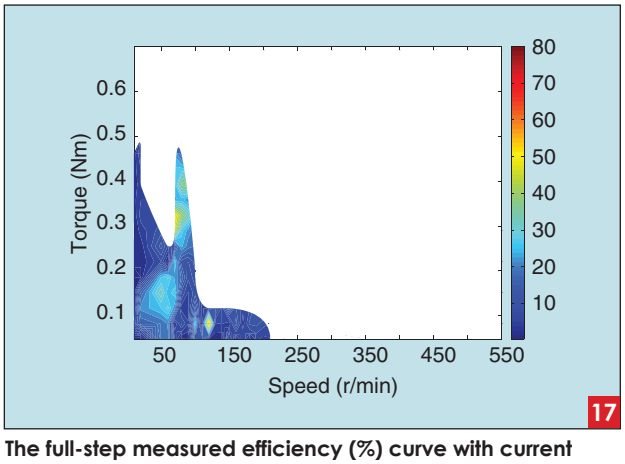


**The full-step measured efficiency (%) curve with current reduction.**

Another interesting issue is the accordance between the estimated optimal current based on (5) and the measured minimal current on the testbench. Due to the impact of parasitic effects, such as vibrations and inertia, the motor will not be able to operate at the predicted optimal current values for every operating point. However, Table 1 shows that the equation to predict the possible current

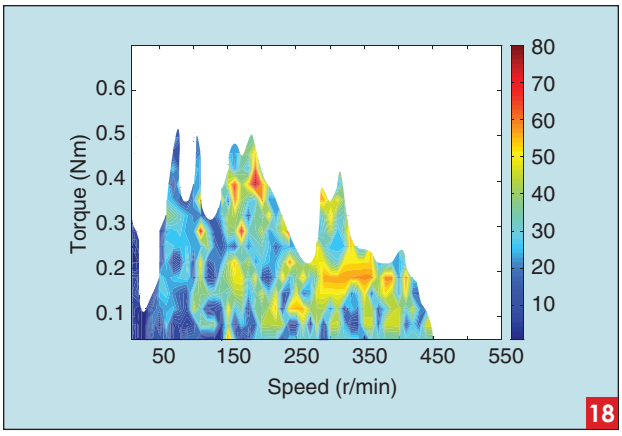


**The half-step measured efficiency (%) curve with current reduction.**

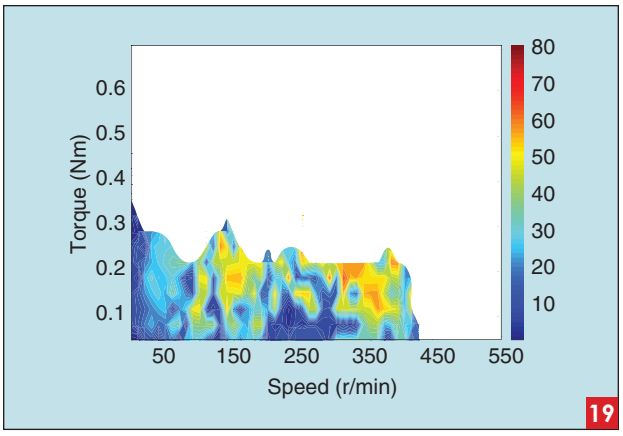


**The microstep measured efficiency (%) curve with current reduction.**

**TABLE 1. SOME EFFICIENCIES AND POSSIBLE CURRENT REDUCTION.**

| | Speed (r/min) | Torque (Nm) | Efficiency (%) | Measured Minimum/Optimal Current (%) | Predicted Minimum/Optimal Current (%) |
|---|---|---|---|---|---|
| Full step | 50 | 0.04 | 13.1 | 53.2 | 52.8 |
| | 70 | 0.04 | 27.0 | 74.5 | 52.2 |
| | 160 | 0.04 | 13.3 | 42.6 | 49.1 |
| Half step | 70 | 0.04 | 9.7 | 53.2 | 63.2 |
| | 290 | 0.2 | 35.5 | 42.6 | 41.2 |
| | 420 | 0.04 | 16.6 | 32.0 | 53.9 |
| Microstep | 70 | 0.24 | 17.7 | 31.9 | 32.6 |
| | 250 | 0.24 | 69.0 | 31.9 | 27.0 |
| | 380 | 0.12 | 30.7 | 42.6 | 37.3 |

reduction could be used if a safety margin is considered. When a safety margin of 20% is added to the estimated optimal current, to determine the current level, the motor will be able to operate at the given operating points. However, at half-step operation, problems could still occur due to a large torque ripple, as shown on the right side of Figure 4(b).

### *Vector Control*

The vector control principle is based on the optimization of the torque/current ratio. The measurements shown in Figure 20 prove that this approach increases the efficiency to a more optimal level. Nevertheless, at lower torques and speed setpoints, the efficiency is still low due to the low useful mechanical power. However, for the largest part of the map, the efficiency varies around 45%. Compared with the efficiencies obtained with half- and microstepping control

**TABLE 2. THE MEASURED EFFICIENCIES FOR FIVE DIFFERENT STEPPING MOTORS.**

| | | | | | | |
|---|---|---|---|---|---|---|
| Motor data | Stator phase-resistance (Ω) | 7.75 | 0.8 | 0.5 | 0.6 | 0.65 |
| | Torque constant (Nm/A) | 0.62 | 0.17 | 0.16 | 0.38 | 0.63 |
| | Nominal current $I_{nom}$ (A) | 0.9 | 3 | 4.7 | 4.7 | 4 |
| | Dimensions (flange × length) | □42 × 44.5 | □42 × 77 | □57.5 × 55 | □57.5 × 77 | ○71 × 77 |
| | Full-step efficiency at maximum output power* (%) | 39.9 | 25.4 | 18.5 | 27.6 | 33.9 |
| | Optimized microstep efficiency at n = 170 r/min, $T_{load}$ = 0.2 Nm (%) | 55.2 | 49.7 | 66.0 | 54.4 | 64.4 |
| | Relative motor load at n = 170 r/min, $T_{load}$ = 0.2 Nm (%) | 142 | 100 | 85 | 50 | 42.5 |

□ Square motor.
○ Circular motor.

at minimized current, the gain in efficiency can be as high as 62% using the vector control algorithm.

Because of the vector control structure, this optimized torque/current ratio does not affect the dynamic behavior and margin for torque or speed setpoint disturbances. Furthermore, Figure 20 clearly shows that the area in which the stepping motor is able to deliver torque at a certain speed setpoint is much larger compared with the full-, half-, and microstepping control because of the smoother movement obtained by the vector control principle. Figure 21 shows an overview and compares the efficiencies at 90 r/min (18% $n_{max}$) and 0.1862 Nm (30% $T_{max}$) for full-, half-, and microstepping and vector control.

FOR LOW-SPEED SETPOINTS AND LOAD TORQUES, THE CURRENT COULD BE REDUCED SIGNIFICANTLY.

### *Influence of Motor Parameters*

A motor with a stator resistance of 0.5 Ω and a nominal current of 4.7 A is used for all of the previous measurements. To have an insight on the influence of the stepping motor parameters on the efficiency, the efficiencies are measured for five different two-phase hybrid stepping motors. The full-step efficiency is measured for each motor at the operating point with a maximum output power. Another interesting operating point to compare the motors is at $n = 170$ r/min and $T_{load} = 0.2$ Nm for a microstep operation because all of the selected motors can operate at that particular load and speed. These results are depicted in Table 2. It can be seen that there is a clear correlation between the full-step efficiency at the maximum output power and the torque constant of the motor. Moreover, the copper losses, which are dominant, are determined by the product of the stator phase resistance and the square of the current. Hence, the nominal current, resistance, and torque constant are the most important motor parameters to determine the efficiency.

## Conclusions

For the full-, half-, and microstep control of a two-phase hybrid stepping motor, a detailed overview of the efficiency is given using isoefficiency curves. These curves are obtained by a theoretical approach and through measurements.

The measurement results give the most accurate idea of the efficiency of the stepping motor driven by different drive algorithms. As the basic idea of this article is to illustrate the trends and principles of the energy efficiency and the impact of the drive algorithm on that efficiency, the accuracy of the measurements was not addressed. However, the test rig is built with high-accuracy components to keep the measurement errors minimal. It is shown that the theoretical efficiency could be predicted easily and accurately by only considering copper losses. A maximum deviation between the measured and the calculated efficiency of 3.5% is observed. However, this theoretical approach is interesting because it shows that an easy calculation is enough to give a more or less accurate idea of the efficiency and losses.

The bulk of the stepping motor applications is driven in open loop, with a maximum current to avoid step loss. Therefore, these drive strategies result in a very poor efficiency. To increase the efficiency, the current can be reduced. The possible current reduction depends on the operating point in the torque–current area. As a result, the efficiency can be significantly increased by up to nine times. This current reduction approach is achievable on most basic stepping motor drives. Moreover, this article proposed a simple formula to estimate the optimal current. The measurements showed that, when a safety margin of 20% is added to this optimal current, the user can be sure that the stepping motor will operate at the desired speed and load torque.

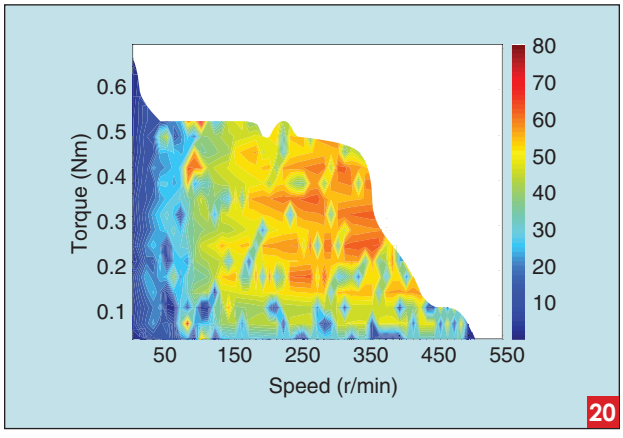


**The vector control measured efficiency curve (%).**

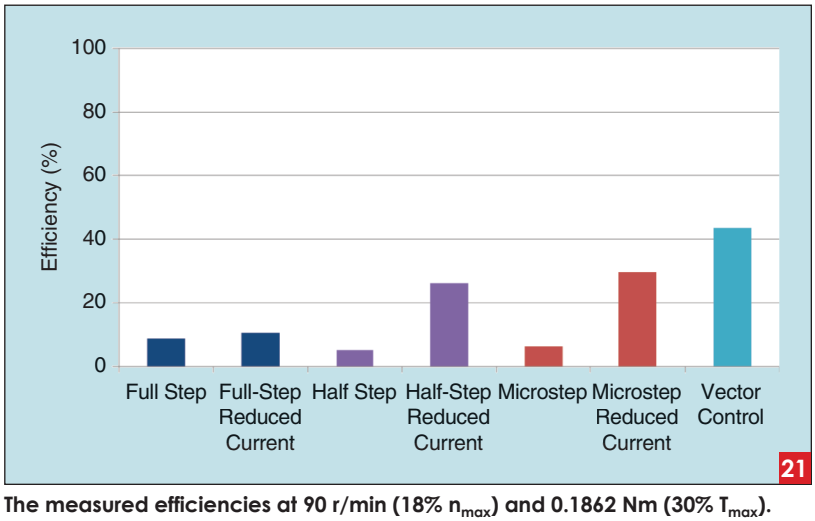


**The measured efficiencies at 90 r/min (18% $n_{max}$) and 0.1862 Nm (30% $T_{max}$).**

The proposed vector control algorithm not only increases the efficiency (sometimes up to 62%) but also results in a much larger area in which the system is able to deliver a certain torque at a particular speed setpoint. Furthermore, the dynamic behavior and margin for the torque and speed setpoint disturbances is not influenced by optimizing the torque/current ratio using the vector control algorithm. On the other hand, the current reduction approach used for full, half, and microstepping implies that there is no margin left for torque or speed disturbances. In addition, it should be noted that all of the algorithms discussed in this article can be implemented without any additional hardware cost, apart from the controller. The vector control algorithm requires position information, which can be estimated by means of a sensorless algorithm. However, implementing a sensorless algorithm in a stepping motor drive is not common due to the computational complexity. Moreover, most commercial stepping motor drives do not provide the current and voltage measurements.

Furthermore, the efficiency of different stepping motors is compared. A clear correlation is observed between the efficiency, on one hand, and the nominal current, stator resistance, and torque constant, on the other hand.

## References


[1] S. Derammelaere, B. Vervisch, J. Cottyn, F. De Belie, B. Vanwalleghem, K. Stockman, L. Vandevelde, P. Cox, and G. Van den Abeele, "ISO efficiency curves of a two-phase hybrid stepping motor," in *Proc. IEEE Industry Applications Society Annu. Meet.*, 2010, pp. 1–5.

[2] E. B. Agamloh, "The partial-load efficiency of induction motors," *IEEE Trans. Ind. Applicat.*, vol. 45, no. 1, pp. 332–340, 2009.

[3] M. J. Melfi, "Quantifying the energy efficiency of motors on inverters," *IEEE Ind. Applicat. Mag.*, vol. 17, no. 6, pp. 37–43, 2011.

[4] W. Finley, B. Veerkamp, D. Gehring, and P. Hanna, "Improving motor efficiency levels globally," *IEEE Ind. Applicat. Mag.*, vol. 15, no. 1, pp. 39–49, 2009.

[5] E. B. Agamloh, "Induction motor efficiency," *IEEE Ind. Applicat. Mag.*, vol. 17, no. 6, pp. 20–28, 2011.

[6] ROHM Semiconductor, Selecting stepper motor drivers for optimum performance, White Paper, California, San Diego. [Online]. Available: http://www.rohm.com/documents/11308/12928/ROHM-SMD-WP.pdf

[7] B. Robert, F. Alin, and C. Goeldel, "Aperiodic and chaotic dynamics in hybrid step motor-new experimental results," in *Proc. ISIE IEEE Int. Symp. Industrial Electronics*, 2001, vol. 3. pp. 2136–2141.

[8] J. Reiss, B. Robert, F. Alin, and M. Sandler, "Flip phenomena and coexisting attractors in an incremental actuator," in *Proc. IEEE Int. Conf. Industrial Technology*, 2003, vol. 2, pp. 866–870.

[9] M. Bodson, J. S. Sato, and S. R. Silver, "Spontaneous speed reversals in stepper motors," *IEEE Trans. Control Syst. Technol.*, vol. 14, no. 2, pp. 369–373, 2006.

[10] K. Inaba, Y. Noda, T. Miyoshi, K. Terashima, M. Nishida, and N. Suganuma, "Driving control considering torsional vibration suppression in a stepping motor with a full-step drive," in *Proc. IECON 35th Annu. IEEE Industrial Electronics Conf.,* 2009, pp. 1116–1121.

[11] W. Kim, J. Han, I. Choi, and C. C. Chung, "Velocity ripple minimization in permanent magnet stepper motor using current error based iterative learning control," in *Proc. ICCAS-SICE*, 2009, pp. 598–602.

[12] Q. N. Le and J.-W. Jeon, "Neural-network-based low-speed-damping controller for stepper motor with an FPGA," *IEEE Trans. Ind. Electron.*, vol. 57, no. 9, pp. 3167–3180, 2010.

[13] K. W.-H. Tsui, N. C. Cheung, and K. C.-W. Yuen, "Novel modeling and damping technique for hybrid stepper motor," *IEEE Trans. Ind. Electron.*, vol. 56, no. 1, pp. 202–211, Jan. 2009.

[14] H. Gao, S. Cheng, L. Sun, and E. Kang, "Maximum torque/current control of 2-phase hybrid stepping motor," in *Proc. IEEE Int. Electric Machines Drives Conf.*, 2003, vol. 3, pp. 1781–1786.

[15] W. Kim, C. Yang, and C. C. Chung, "Design and implementation of simple field-oriented control for permanent magnet stepper motors without DQ transformation," *IEEE Trans. Magn.*, vol. 47, no. 10, pp. 4231–4234, 2011.

[16] A. Piippo, M. Hinkkanen, and J. Luomi, "Adaptation of motor parameters in sensorless PMSM drives," *IEEE Trans. Ind. Applicat.*, vol. 45, no. 1, pp. 203–212, 2009.

[17] Y.-D. Yoon, S.-K. Sul, S. Morimoto, and K. Ide, "High-bandwidth sensorless algorithm for ac machines based on square-wave-type voltage injection," *IEEE Trans. Ind. Applicat.*, vol. 47, no. 3, pp. 1361–1370, 2011.

[18] P. Garcia, F. Briz, M. W. Degner, and D. Diaz-Reigosa, "Accuracy, bandwidth, and stability limits of carrier-signal-injection-based sensorless control methods," *IEEE Trans. Ind. Applicat.*, vol. 43, no. 4, pp. 990–1000, 2007.

[19] L. Weijie and Z. Zhuo, "Simulation and experiment of sensorless direct torque control of hybrid stepping motor based on DSP," in *Proc. 2006 IEEE Int. Conf. Mechatronics Automation*, 2006, pp. 2133–2138.

[20] J. De Leon-Morales, R. Castro-Linares, and O. H. Guevara, "Observer-based controller for position regulation of stepping motor," *IEE Proc.-Control Theory Applicat.*, vol. 152, no. 4, pp. 465–476, 2005.

[21] W. Kim and C. C. Chung, "Novel position detection method for permanent magnet stepper motors using only current feedback," *IEEE Trans. Magn.*, vol. 47, no. 10, pp. 3590–3593, 2011.

[22] S. Derammelaere, B. Vervisch, F. De Belie, J. Cottyn, G. Van den Abeele, P. Cox, K. Stockman, and L. Vandevelde, "A nonlinear and linear model of a hybrid stepping motor," in *Proc. ELECTRIMACS*, 2011, pp. 1–6.

[23] C. Kuert, M. Jufer, and Y. Perriard, "New method for dynamic modeling of hybrid stepping motors," in *Proc. 37th Industry Applications Society Annu. Meet.,* 2002, vol. 1, pp. 6–12.

[24] S. Williamson, M. Lukic, and A. Emadi, "Comprehensive drivetrain efficiency analysis of hybrid electric and fuel cell vehicles based on motor-controller efficiency modeling," *IEEE Trans. Power Electron.*, vol. 21, no. 3, pp. 730–740, 2006.

[25] K. Stockman, S. Dereyne, D. Vanhooydonck, W. Symens, J. Lemmens, and W. Deprez, "Isoefficiency contour measurement results for variable speed drives," in *Proc. 19th Int. Conf. Electrical Machines*, 2010, pp. 1–6.

[26] W. Deprez, J. Lemmens, D. Vanhooydonck, W. Symens, K. Stockman, S. Dereyne, and J. Driesen, "Isoefficiency contours as a concept to characterize variable speed drive efficiency," in *Proc. 19th Int. Conf. Electrical Machines*, 2010, pp. 1–6.

[27] D. Vanhooydonck, W. Symens, W. Deprez, J. Lemmens, K. Stockman, and S. Dereyne, "Calculating energy consumption of motor systems with varying load using iso efficiency contours," in *Proc. 19th Int. Conf. Electrical Machines*, 2010, pp. 1–6.

[28] B. Robert and M. Feki, "Control of the stepping motor," in *Control of Non-Conventional Synchronous Motors*, J. P. Louis, Ed. New York: Wiley-ISTE, 2011.

[29] B. C. Kuo, *Incremental Motion Control—Step Motors and Control Systems*. Champaign, IL: SRL Publishing Company, 1979.

[30] S. Derammelaere, B. Vervisch, F. De Belie, J. Cottyn, G. Van den Abeele, P. Cox, K. Stockman, and L. Vandevelde, "Sensitivity analysis of a linear model for a vector controlled hybrid stepping motor," in *Proc. 2010 19th Int. Conf. Electrical Machines*, 2010, pp. 1–5.

[31] P. Acarnley, *Stepping Motors: A Guide to Theory and Practice*, 4th ed. London: The Institution of Engineering and Technology, 2007, p. 159.



*Stijn Derammelaere, Bram Vervisch, Johannes Cottyn, Bart Vanwalleghem, Frederik De Belie, Kurt Stockman, and Lieven Vandevelde are with Ghent University in Belgium. Peter Cox is with ON Semiconductor in Belgium. Griet Van Den Abeele is with PsiControl Mechatronics in Belgium. This article first appeared as "ISO Efficiency Curves of a Two-Phase Hybrid Stepping Motor" at the 2010 IEEE IAS Annual Meeting.*